

Effects of stress on the evolution of Σ -shaped dislocation arrays in a 4H-SiC epitaxial layer

Cite as: J. Appl. Phys. 129, 245101 (2021); doi: 10.1063/5.0048195

Submitted: 20 February 2021 · Accepted: 8 June 2021 ·

Published Online: 25 June 2021



View Online



Export Citation



CrossMark

Moonkyong Na,^{1,a)} Wook Bahng,¹ Hyemin Jang,^{1,2} Jung Min Kim,³ and Hyundon Jung³

AFFILIATIONS

¹ Power Apparatus Research Division, Korea Electrotechnology Research Institute, 12, Jeongui-gil, Seongsan-gu, Changwon-si, Gyeongsangnam-do 51543, Republic of Korea

² Department of Materials Science and Engineering, Pusan National University, 2, Busandaehak-ro 63 beon-gil, Geumjeong-gu, Busan 46241, Republic of Korea

³ Etamax Co., Ltd., 280-17, Saneop-ro 155 Beon-gil, Gwonneon-gu, Suwon-si, Gyeonggi-do 16648, Republic of Korea

^{a)}Author to whom correspondence should be addressed: nmk@keri.re.kr

ABSTRACT

Five Σ -shaped dislocation arrays in 100-mm-diameter, 12- μm -thick 4H-SiC epitaxial wafers were observed using photoluminescence mapping. The structure of the Σ -shaped dislocation arrays was characterized using nondestructive analytical techniques of photoluminescence mapping, microphotoluminescence spectroscopy, and x-ray topography. Each Σ -shaped dislocation array consists of two basal plane dislocations (BPDs) at the interfacial dislocation terminal points and two half-loop arrays. The interfacial dislocation pairs nucleate from BPDs in the substrate. Three independent stresses lead to interfacial dislocations: thermal stress (τ_T), stress induced by misfit strain (τ_M), and interaction force (τ_I). The main cause of interfacial dislocation formation is attributed to the development of τ_T within the wafer due to temperature nonuniformity. τ_M and τ_I also contribute to the formation of interfacial dislocations. Larger stresses increase the BPD glide velocity in the interfacial dislocations, thereby producing longer Σ -shaped dislocation arrays.

Published under an exclusive license by AIP Publishing. <https://doi.org/10.1063/5.0048195>

I. INTRODUCTION

Silicon carbide (SiC) is an attractive semiconductor for high-power, high-temperature, and high-frequency electronic devices due to its wide bandgap, high-breakdown electric field, and high thermal conductivity.^{1,2} The growth technologies of single crystal and epitaxial layer SiC have greatly developed so that 6-in.-diameter SiC epitaxial wafers are now commercially available. However, the presence of extended defects has hampered the development of SiC semiconductor devices.^{3–7} Most of these defects in an epitaxial layer propagate from the substrate. Among them, most (>95%) of the basal plane dislocations (BPDs) in the substrate convert without any special treatment to threading edge dislocations (TEDs) within a few micrometers of the initial epitaxial layer.⁸ The BPD density in an SiC epitaxial layer can be reduced to 0.1–1.0 cm^{−2}.^{9,10} Interfacial dislocations form when BPDs glide along the substrate/epitaxial layer interface. They occasionally form half-loop arrays (HLAs) and BPDs in epitaxial layers.¹¹ The formation mechanism of interfacial dislocations has been studied extensively. The main cause of interfacial dislocation is

thermal stress (τ_T), which induces the formation of interfacial dislocations at a given annealing temperature if the temperature gradient across the epitaxial wafer exceeds a critical value.^{12–14} Jacobson *et al.* suggested that interfacial dislocations are misfit dislocations caused by misfit strain between different doping concentrations of the substrate and epitaxial layer.¹⁵ Zhang *et al.* found that interfacial dislocation densities and BPD densities in the substrate were correlated.¹⁶ Most interfacial dislocations are connected at one end to a BPD in the substrate and at the other end to another BPD continuing toward the epitaxial layer surface. Wang *et al.* studied interfacial dislocation pairs and determined how they evolved from BPDs.¹⁷

The BPDs included in the interfacial dislocation or the basal plane segment of an HLA expand to stacking faults under high current stress or ultraviolet (UV) irradiation. This process leads to a reduction in device performance via bipolar degradation.¹⁸ The increasing demand for high-powered SiC-based devices requires lower doping concentration of the epitaxial layer with increasing epitaxial layer thickness.^{19,20} This increases the difficulty of the epitaxial growth process in terms of maintaining temperature uniformity and

low doping concentration throughout the wafer. In addition, low-resistivity substrates are favorable for fabrication of devices having low on-state resistance. It is difficult to maintain constant temperature throughout the wafer during thick epitaxial layer growth. Furthermore, the doping concentration difference between the substrate and epitaxial layer increases. These behaviors during epitaxial growth act as stresses from which interfacial dislocations evolve. It is important to detect defects in a SiC epitaxial layer using nondestructive approaches before device processing.

Herein, we observed Σ -shaped dislocation arrays using photoluminescence (PL) mapping. The formation of these Σ -shaped dislocation arrays was studied using nondestructive techniques to examine in detail the effect of τ_B , stress induced by misfit strain (τ_M), and interaction force (τ_I).

II. EXPERIMENTAL

A commercially available 100-mm-diameter 4H-SiC epitaxial wafer was used in this study. The 12- μm -thick epitaxial layer was doped with nitrogen at $7 \times 10^{15} \text{ cm}^{-3}$. The off-cut angle was 4° in the $[11\bar{2}0]$ direction. The nondestructive techniques of PL mapping, microphotoluminescence (μ -PL) spectroscopy, and synchrotron white beam x-ray topography (SWBXRT) were used to investigate the defect structures. PL mapping was performed using an EtaMax MiPLATO-SiC[®] instrument at 355 nm with a 25 mW laser. Images were simultaneously collected from four different bandpass filters as the entire 100-mm-diameter wafer was rotated at 1800 rpm. The scan step size was 5 μm . Dislocations were nondestructively imaged using intensity differences in the PL signal. μ -PL spectroscopy measurements were performed at 325 nm with a 25 mW He-Cd laser. The scan step size was 2 or 20 μm and the exposure time was 50 ms at the specific measurement region. XRT was performed using the PLS-II 9D beamline at the Pohang Accelerator Laboratory (PAL). Defect structures were identified from reflection topography images along the $g = \bar{1}\bar{1}28$ diffraction vector. The incidence x-ray energy ranged from 4 to 35 keV and the photon flux was 10^{11} – 10^{12} photons per second. The penetration depth of the x-rays was controlled by varying the x-ray angle of incidence and estimated using the x-ray mass attenuation coefficients of SiC in consideration of the XRT geometry.²¹ Diffraction images were recorded on high-resolution AGFA Structurix D3-SC films.

III. RESULTS AND DISCUSSION

A. Observation of Σ -shaped dislocation arrays

Five Σ -shaped dislocation arrays (#1–5) were observed within the 100-mm-diameter 4H-SiC epitaxial wafer by PL mapping (Fig. 1). The numbering of the Σ -shaped dislocation arrays increases with distance from the wafer center. Five Σ -shaped dislocation arrays were distributed along the radial direction from the wafer center. Two additional interfacial dislocations (D and S) were also observed.

Figure 2(a) shows a representative PL mapping image of the #2 Σ -shaped dislocation array; PL mapping images of all five Σ -shaped dislocation arrays can be found in Fig. S1 in the supplementary material. Figure 2(b) shows an x-ray topography

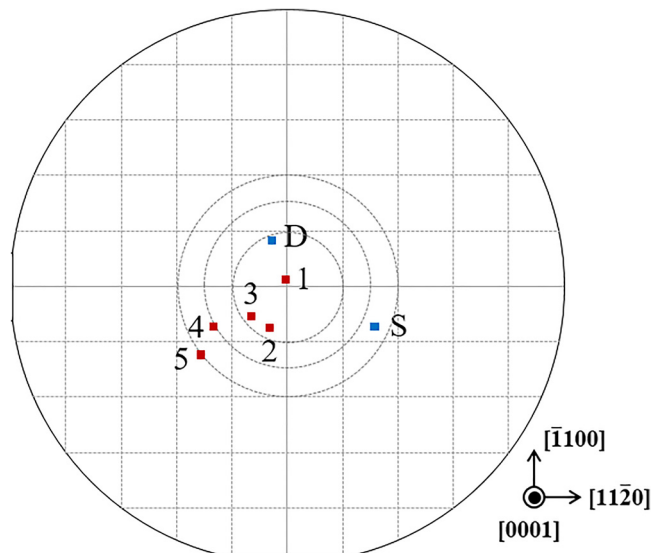


FIG. 1. Distribution of five (#1–5) Σ -shaped dislocation arrays and two interfacial dislocations (denoted as D and S) within the wafer.

(XRT) image of the #2 Σ -shaped dislocation array, which consisted of interfacial dislocation pairs (open white arrows) and HLAs (open black arrow) (XRT images of all five Σ -shaped dislocation arrays can be found in Fig. S2 in the supplementary material). HLAs formed via interactions between the surface and the end segments of gliding BPDs during epitaxial growth. BPDs were observed at the terminal points of interfacial dislocations (filled black arrows). Other BPDs connected with interfacial dislocations at the curved segments (filled white arrows). The interfacial dislocation pairs (open white arrows) and BPDs (filled white arrows) were absent in PL mapping images because they were located at the substrate/epitaxial layer interface and substrate [Fig. 2(a)]. PL analysis did not detect any particular signals at the highly doped substrate due to the very short carrier lifetime.²² The HLAs (open black arrows) and BPDs in the epitaxial layer (filled black arrows) were observed in PL mapping images, and the defects were Σ -shaped. The presence of HLAs was confirmed by μ -PL spectroscopy (Fig. 6). Threading screw dislocations (TSDs) and TEDs were recorded as dark spots in the PL maps [Fig. 2(a)]. The large white spots about 40 μm in diameter in Fig. 2(b) correspond to TSDs while the small ones about 20 μm in diameter correspond to TEDs. The dark lines in Fig. 2(b) correspond to BPDs; they are absent in the PL map in Fig. 2(a) because they were located in the substrate.

The length of each interfacial dislocation in the five Σ -shaped dislocation arrays was plotted as a function of their distance from the wafer center (Fig. 3). When the interfacial dislocation is along $[\bar{1}100]$, the direction is upward, and when it is along $[1\bar{1}00]$, the direction is downward. The length of each interfacial dislocation increased with proximity to the center of the wafer. In the #1 Σ -shaped dislocation array, the length of the upward direction interfacial dislocation was 1232 μm while that of the downward

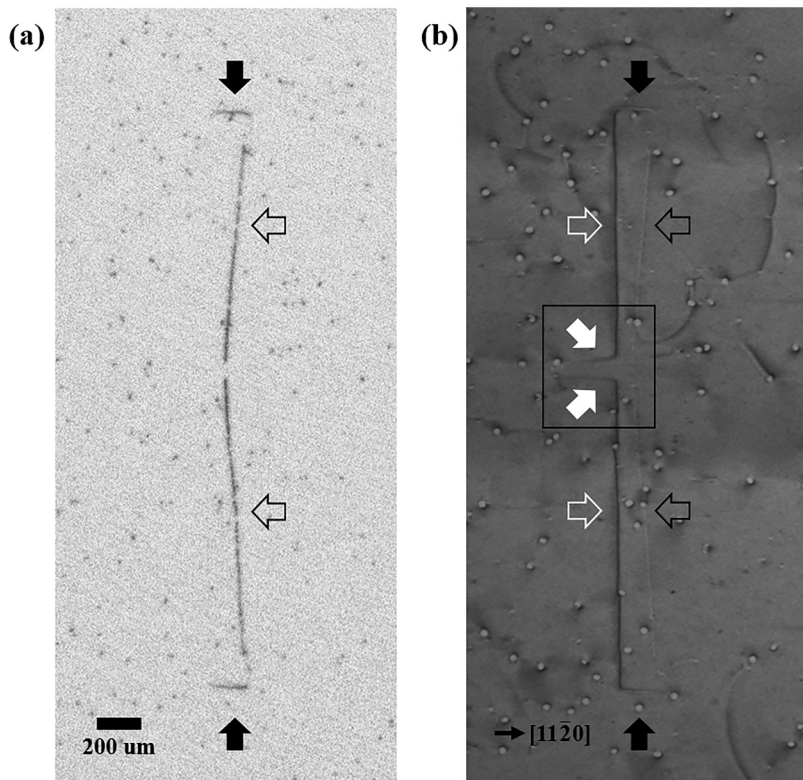


FIG. 2. (a) Photoluminescence mapping image at the band edge emission and (b) x-ray topography image of the #2 Σ -shaped dislocation array consisted of interfacial dislocation pairs (open white arrows), half-loop arrays (open black arrows), basal plane dislocations in the substrate (filled white arrows), and basal plane dislocations at the terminal point of interfacial dislocation (filled black arrows).

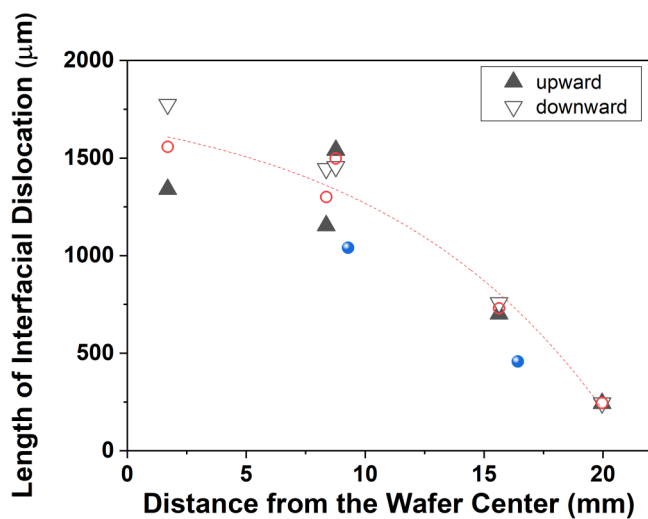


FIG. 3. Length of interfacial dislocation pairs gliding (a) upward (filled triangles) and (b) downward (open triangles) as a function of distance from the wafer center. The average values of two interfacial dislocation lengths (open circles) and the estimated values are shown in red. The filled blue circles indicate the length of each interfacial dislocation pair.

direction case was $1620 \mu\text{m}$, i.e., the interfacial dislocation length was shorter further away from the center. The lengths of the interfacial dislocation in the upward and downward directions were 243 and $245 \mu\text{m}$, respectively, in the #5 Σ -shaped dislocation array. No Σ -shaped dislocation array was observed further than 20 mm from the wafer center. The average interfacial dislocation pair length is denoted as a red open circle in the figure; the length gradually decreased with increasing distance from the wafer center. The filled blue circles correspond to the lengths of the D and S interfacial dislocations, which were 1040 and $457 \mu\text{m}$, respectively [Figs. 4(a) and 4(b)]. HLAs were observed in D interfacial dislocations [Fig. 4(a)] but not in S interfacial dislocations [Fig. 4(b)]. Regardless of the HLA formation, the D and S interfacial dislocation lengths were shorter than the average interfacial dislocation pair length. A D interfacial dislocation was a pair at the initial stage of interfacial dislocation formation; two BPDs glided in opposite directions, but one BPD was terminated at the initial stage of gliding at the substrate epitaxial layer interface. This presumed interaction between dislocations requires further study.

Figure 5 shows a magnified XRT image of a parallel BPD pair connected with interfacial dislocations at the curved segments in the #2 Σ -shaped dislocation array shown in Fig. 2(b) (black rectangle). The BPD pair was observed as a function of x-ray penetration depth in the SiC epitaxial wafer. The calculated penetration depth of the x-rays in Fig. 5(a) was less than $10 \mu\text{m}$. The image of the BPD pair

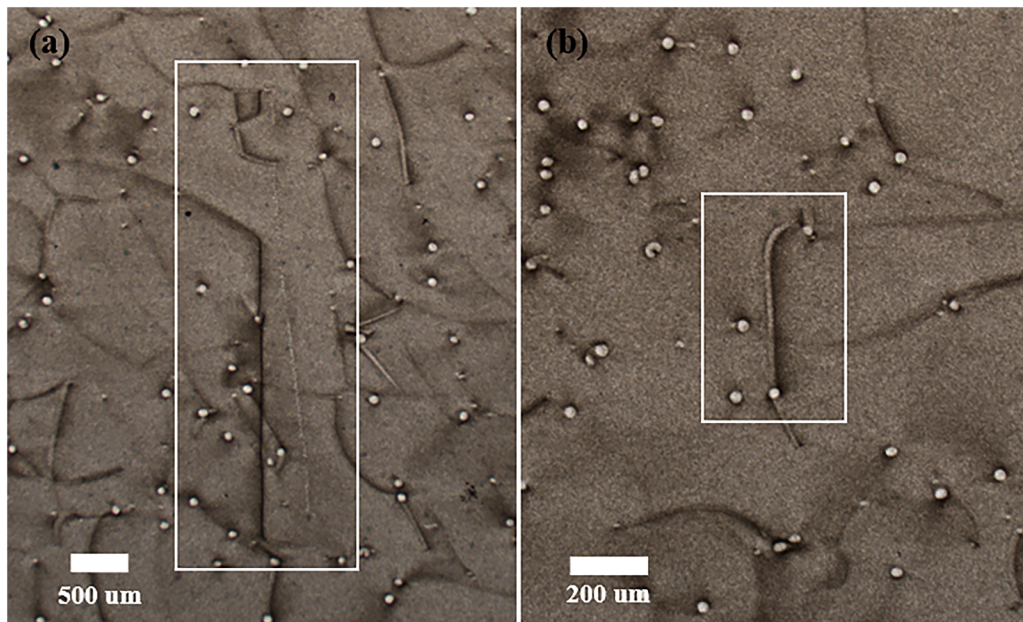


FIG. 4. X-ray topography images of (a) D and (b) S interfacial dislocations; $g = \bar{1}\bar{1}28$.

denoted A and B became clearer with increasing x-ray penetration depth to 15 and 36 μm [Figs. 5(b) and 5(c)]. This indicated that the BPD pair was present in the substrate, which explained the absence of BPDs in the PL mapping image of Fig. 2(a). The interfacial dislocation pairs were caused by gliding of pre-existing BPD in the

substrate. The BPD pair and the interfacial dislocation pair had the same Burgers vectors. Each interfacial dislocation pair in a Σ-shaped dislocation array expanded in the direction opposite to the perpendicular [1120] direction, which meant that the two BPDs in an interfacial dislocation pair had opposite signs.

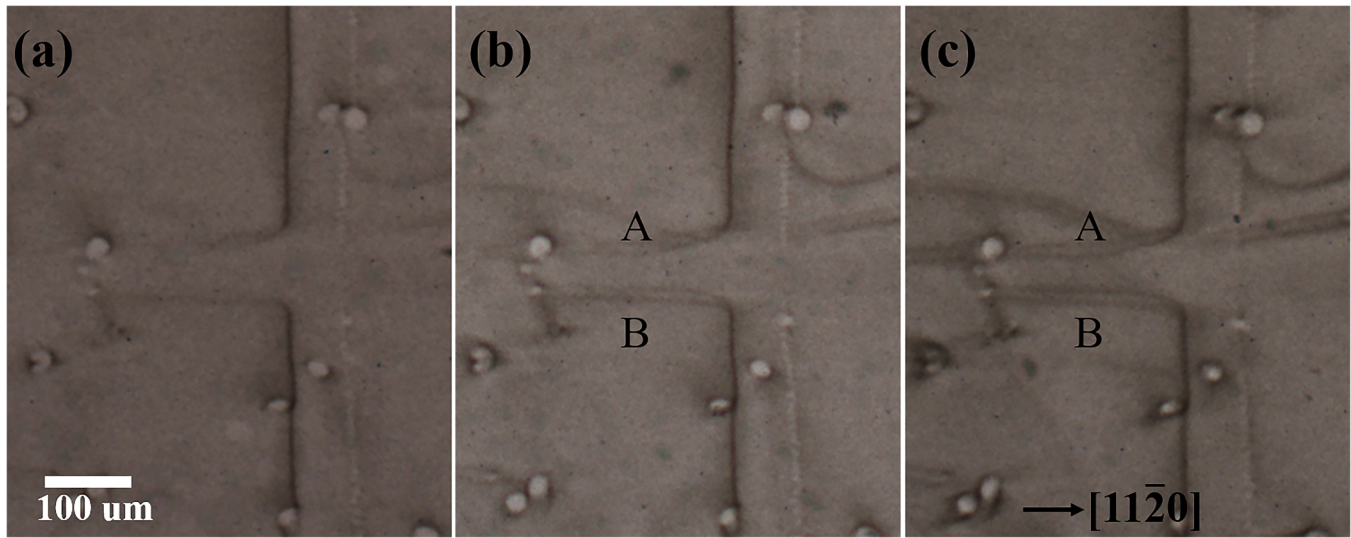


FIG. 5. Magnified x-ray topography images of basal plane dislocation pairs connected with the #2 Σ-shaped dislocation array at calculated x-ray penetration depths of (a) less than 10 μm, (b) 15 μm, and (c) 36 μm; $g = 1128$.

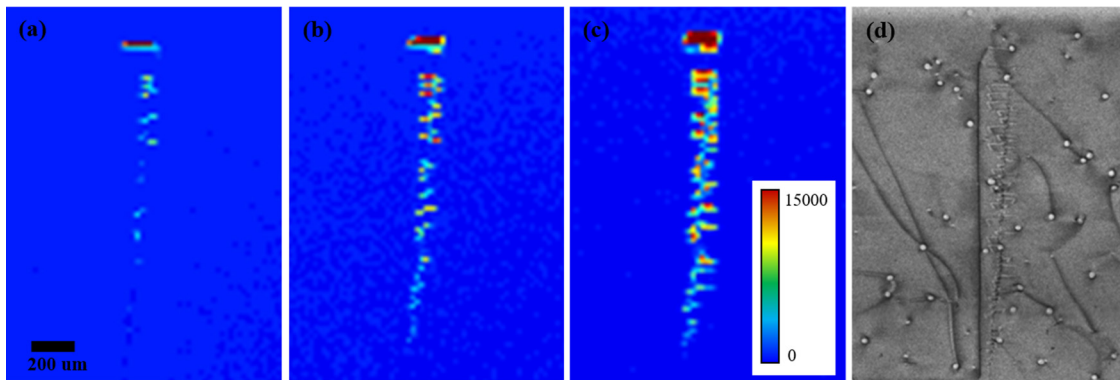


FIG. 6. Microphotoluminescence (μ -PL) intensity mapping images at a fixed wavelength of 420 nm. Expansion of Shockley-type stacking faults (3, 1) from basal plane segments in the half-loop arrays after (a) one, (b) two, and (c) three consecutive μ -PL measurements. (d) Partial dislocations of Shockley-type stacking faults observed by x-ray topography after three consecutive μ -PL measurements.

Expansion of basal plane segments in HLAs to Shockley-type stacking faults (3, 1) after UV irradiation was observed by μ -PL spectroscopy at a fixed wavelength of 420 nm (Fig. 6). UV irradiation was insufficient to cause expansion of basal plane segments during PL mapping measurements when the wafer was rotated at 1800 rpm. Stacking fault expansion was not observed after three consecutive PL mapping measurements. The UV exposure time was intentionally increased to observe the expansion of basal plane segments in HLAs during μ -PL spectroscopy measurements. The basal plane segments were located on the same basal plane as the BPD at the end of the interfacial dislocation. The expansion of basal plane segments to stacking faults (3, 1) under UV irradiation is well-known.²³ During repeated UV exposure, the stacking faults (3, 1) continued to expand. Partial dislocations were observed in each Shockley-type stacking fault (3, 1) using XRT after three consecutive μ -PL spectroscopy measurements [Fig. 6(d)].

B. Distribution and origin of interfacial dislocation pairs

Several types of stresses could affect the formation of interfacial dislocations during epitaxial growth. Temperature nonuniformity can cause τ_T . A second influence is τ_M due to the difference in doping concentration between the substrate and the epitaxial layer. The last effect is τ_I between dislocations. The total stress, τ_{tot} , which can affect the formation of an interfacial dislocation during epitaxial growth, can be described by Eq. (1) as follows:

$$\tau_{tot} = \tau_T + \tau_M + \tau_I, \quad (1)$$

where τ_T is the thermal stress induced by the radial temperature gradient, τ_M is the stress induced by misfit strain due to the difference in nitrogen doping concentration between the substrate and the epitaxial layer, and τ_I is the interaction force induced by interaction between dislocations. Interfacial dislocations expand when the total elastic stress exceeds the critical resolved shear stress (CRSS) during epitaxial growth.

1. Thermal stress

Thermal stress develops during epitaxial growth when the temperature distribution of the growing surface is nonuniform. Greater τ_T induces a longer interfacial dislocation of the BPD glide.¹³ If the temperature distribution is comparatively uniform throughout the wafer, the CRSS could be devalued to glide the BPDs. The large τ_T easily surpassed the CRSS at the growth temperature and BPDs could glide during epitaxial growth and eventually form interfacial dislocations.¹² The CRSS for slip on the $\langle 11\bar{2}0 \rangle$ (0001) primary slip system in 4H-SiC was determined by Demenet *et al.*²⁴ The CRSS was 4 MPa at 1300 °C. Extrapolating to 1600 °C, which was the presumed epitaxial layer growth temperature, the CRSS was about 1.0 MPa. Based on the dark contrast of interfacial dislocations in XRT image (Fig. 2), it seems that a large compressive τ_T was applied to the center of the wafer during epitaxial growth.¹³ The temperature of the center region of the wafer was higher than the outer region, which induced a large compressive τ_T at the center of the wafer. The distribution of Σ -shaped dislocation arrays will follow the shape of the temperature gradient. Five Σ -shaped dislocation arrays were distributed along the radial direction from the wafer center (Fig. 1), which implies that the temperature gradient was not axisymmetric within the wafer. The contrast of the D interfacial dislocation located at the end of the inclined ellipse shape was dark, which compares with the bright contrast of the S interfacial dislocation [Figs. 4(a) and 4(b)]. Under the large thermal compressive stress, the contrast of interfacial dislocations showed the black contrast. On contrary, white contrast interfacial dislocation were observed with a tensile thermal stress condition.¹³ The oppositely signed τ_T acted between the D and S interfacial dislocations.

2. Stress induced by misfit strain

This stress is due to the difference in doping concentrations between the substrate and the epitaxial layer. High doping of nitrogen in the substrate induces a large misfit strain at the epitaxial layer due to the small lattice contraction effect of nitrogen

TABLE I. Gap and interaction force between basal plane dislocation (BPD) pairs connected in five Σ -shaped dislocation arrays.

Pair	Distance from wafer center (mm)	BPD pair separation (μm)	Interaction force (MPa)
#1	1.7	45	0.27
#2	8.4	75	0.16
#3	8.8	50	0.24
#4	15.6	80	0.15
#5	20.0	44	0.27

as a donor in 4H-SiC. That is the major cause of misfit dislocation generation. To calculate the induced lattice compression due to nitrogen doping, the critical thickness for the formation of misfit dislocations in an epitaxial layer needed to be estimated. The epitaxial layer was doped with nitrogen at $7 \times 10^{15} \text{ cm}^{-3}$ and the thickness was $12 \mu\text{m}$. The doping concentration of the substrate ranged from 3×10^{18} to $5 \times 10^{18} \text{ cm}^{-3}$ according to the Hall effect and noncontact sheet resistance measurements. The misfit strain in the epitaxial layer, f_e , is defined according to Eq. (2) as follows:¹⁵

$$f_e = \frac{a_s - a_e}{a_s}, \quad (2)$$

where a_s and a_e are the lattice constants of the substrate and epitaxial layer, respectively. The critical thickness is a function of the strain induced in the epitaxial layer. The estimated critical thickness for releasing the crystal lattice misfit strain under these epitaxial layer doping conditions was $200\text{--}300 \mu\text{m}$. The τ_M was not large enough to form interfacial dislocations, but it could affect the glide of BPDs at the interface of the substrate/epitaxial layer. The τ_M should be controlled in fabrication of low on-state resistance and high-power devices containing a thick epitaxial layer.

3. Interaction force

Dislocations lying very closely together interact by attraction or repulsion, reducing their total energy. The BPD pair at the Σ -shaped dislocation arrays in the substrate has the same Burgers

vector but opposite sign so that they repel each other. The interaction forces are calculated using Eq. (3) as follows:²⁵

$$F_x = \frac{Gb^2}{2\pi(1-\nu)} \frac{x(x^2-y^2)}{(x^2+y^2)^2}, \quad F_y = \frac{Gb^2}{2\pi(1-\nu)} \frac{y(3x^2-y^2)}{(x^2+y^2)^2}, \quad (3)$$

where F_x is the force in the glide direction and F_y is the force perpendicular to the glide plane, x and y are the distances between two dislocations in each direction, G is the shear modulus at room temperature for 4H-SiC (192 GPa),¹² b is the magnitude of the Burgers vector for 4H-SiC (0.370 nm), and ν is the Poisson's ratio for 4H-SiC (0.214).²⁶ An edge dislocation can move by slip only in the plane containing the dislocation line and its Burgers vector. The component of τ_I that is most important in determining the behavior of the dislocations is F_x . It is assumed that the slip plane is defined by the two BPDs at the substrate/epitaxial layer interface, i.e., $y=0$. The calculated τ_I was in the range of 0.15–0.27 MPa (Table I). Although the #2 and #3 Σ -shaped dislocation arrays were closer within the wafer, the interfacial dislocation length of the #3 Σ -shaped dislocation array was greater due to its larger τ_I than that of the #2 Σ -shaped dislocation array (Fig. 3). Therefore, it meant that interatomic force played an important role in the BPD glide behavior.

The possible three stresses that could affect the glide of BPD during epitaxial growth were considered. BPDs glide when τ_{tot} exceeds the CRSS. According to Zhang *et al.*, the resolved shear stress on interfacial dislocations ranges from 0.6 to 1.2 MPa.¹² In this research, the interfacial dislocations formed at a thickness lower than the estimated critical thickness. The exact growth temperature of the commercial epitaxial wafer used in our experiments is unknown. Nevertheless, if the growth temperature was about 1600 °C, the CRSS would be about 1 MPa. A large compressive τ_T was applied to the center of the wafer during epitaxial growth. Although τ_T is understood to be the main cause of interfacial dislocation formation, τ_M and τ_I are also influential. When the τ_{tot} incorporating the three possible stresses is sufficiently large to surpass the CRSS of BPD glide, interfacial dislocation would expand below the estimated critical thickness during epitaxial growth. The structure of the Σ -shaped dislocation array evolving

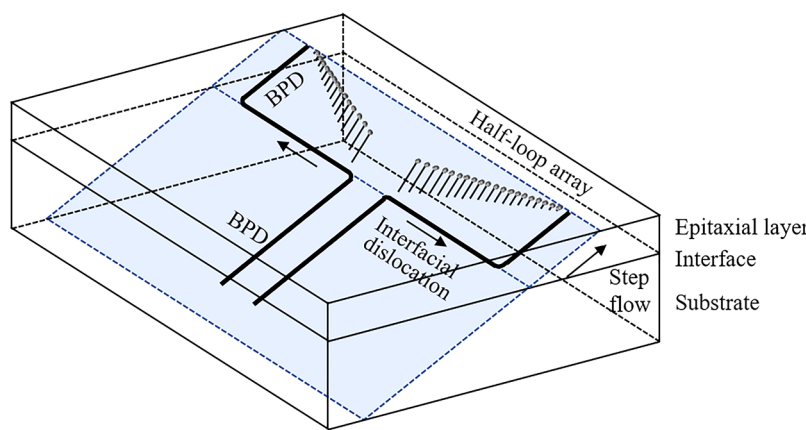


FIG. 7. The schematic drawing for structure of the Σ -shaped dislocation array that evolved under stresses during epitaxy growth.

under stresses during epitaxial growth is depicted in Fig. 7. More and larger Σ -shaped dislocation arrays were observed near the wafer center as τ_{tot} increased. The resolved stress level in the outer region was lower than the CRSS for the glide of BPDs, which resulted in no formation of Σ -shaped dislocation array further than 20 mm from the wafer center.

C. Effect of total stress on BPD glide velocity

The BPD glide velocity in interfacial dislocations can be estimated using the growth rate of the epitaxial layer and the inclination angle of the HLAs. Figure 8(a) shows the change in inclination angle of the HLAs. The #5 Σ -shaped dislocation array, which was the outermost among the Σ -shaped dislocation arrays,

had short HLA lengths of 84 and 152 μm in the upward and downward directions, respectively. Notably, the very short upwardly directed HLA length made it difficult to determine the inclination angle accurately.

The BPD glide velocity, v_g , was calculated according to Eq. (4) as follows:¹²

$$v_g = \frac{v_0}{\tan \theta \tan \alpha}, \quad (4)$$

where v_0 is the growth rate of the epitaxial layer, θ is the inclination angle of the HLAs, and α is the off-cut angle of 4°. The BPD glide velocity is affected by the HLA inclination angle and the fixed epitaxial growth rate and off-cut angle. A lower inclination angle corresponds to a faster BPD glide. Due to the unknown epitaxial layer growth conditions, only relative BPD glide velocities were estimated. For an average BPD glide velocity of the #1 Σ -shaped dislocation array of v_g , the relative BPD glide velocities of #2, 3, 4, and 5 Σ -shaped dislocation arrays were estimated to be $0.66v_g$, $0.63v_g$, $0.54v_g$, and $0.46v_g$, respectively [Fig. 8(b)]. The decreasing BPD glide velocity implies decreasing magnitude of the applied τ_{tot} which was responsible for the glide of BPDs at the substrate/epitaxial layer interface. The glide velocity increased toward the wafer center with increasing magnitude of τ_{tot} . The greater expansion of the interfacial dislocation with increasing BPD glide velocity would result in device performance degradation over a large area.

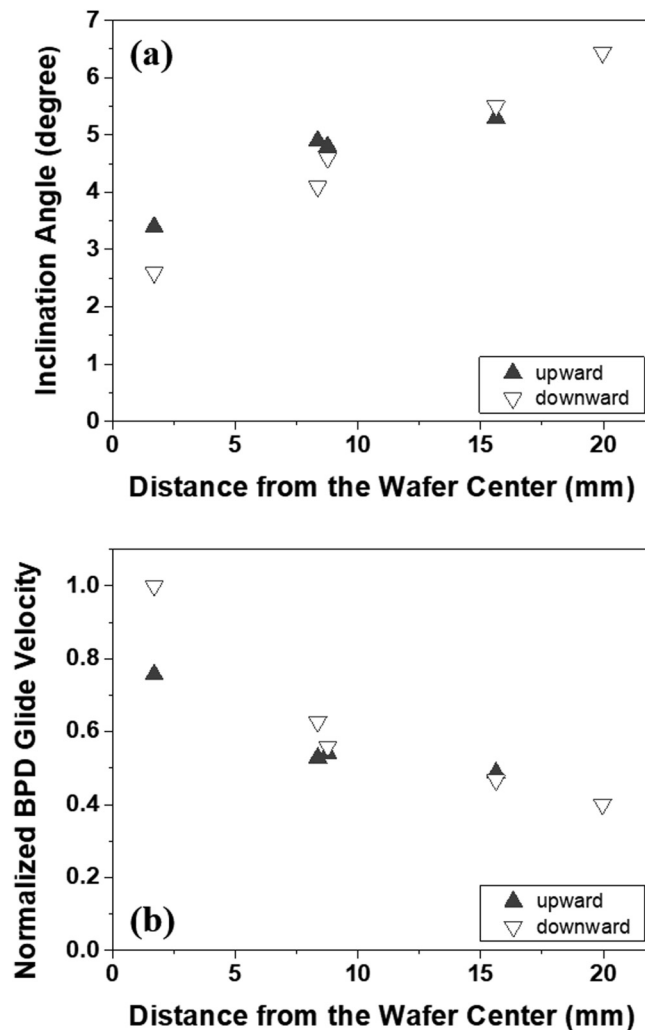


FIG. 8. (a) Inclination angle of half-loop arrays and (b) normalized basal plane dislocation glide velocities in the upward (filled triangles) and downward (open triangles) directions as a function of distance from the wafer center.

IV. CONCLUSIONS

We investigated Σ -shaped dislocation arrays that consisted of interfacial dislocation pairs and two HLAs. BPDs were observed at the terminal points of the interfacial dislocations. The interfacial dislocation pair length in the Σ -shaped dislocation arrays and the BPD glide velocity increased with proximity to the wafer center. The higher temperature of the center region of the wafer compared with that of the outer region induced a large compressive τ_T at the center of the wafer during epitaxial growth. The combination of τ_T , τ_M , and τ_I , i.e., τ_{tot} , surpassed the CRSS of the interfacial dislocations. The BPD glide velocity increased at the substrate/epitaxial layer interface with increasing magnitude of τ_{tot} . The consequent expansion of the HLAs over a wider region in the epitaxial layer would lead to device performance degradation. Maintaining a uniform temperature and reducing misfit strain would mitigate the formation of interfacial dislocations and HLAs and thereby improve the performance and reliability of SiC-powered devices.

SUPPLEMENTARY MATERIAL

See the [supplementary material](#) for photoluminescence mapping images at the band edge emission and x-ray topography images ($g = \bar{1}\bar{1}28$) of all five Σ -shaped dislocation arrays.

ACKNOWLEDGMENTS

This work was supported by the Korea Electrotechnology Research Institute (KERI) Primary Research Program through the National Research Council of Science & Technology (NST) funded by the Ministry of Science and ICT (MSIT) (No. 21A01063).

DATA AVAILABILITY

The data that support the findings of this study are available from the corresponding author upon reasonable request.

REFERENCES

- ¹T. Kimoto and Y. Yonezawa, "Current status and perspectives of ultrahigh-voltage SiC power devices," *Mater. Sci. Semicond. Process* **78**, 43–56 (2018).
- ²A. Agarwal, M. Das, S. Krishnaswami, J. Palmour, J. Richmond, and S.-H. Ryu, "An overview of SiC power devices," *Mater. Res. Soc. Symp. Proc.* **815**, 243 (2004).
- ³Y. Tokuda, I. Kamata, T. Miyazawa, N. Hoshino, T. Kato, H. Okumura, T. Kimoto, and H. Tsuchida, "Glide velocities of Si-core partial dislocations for double-Shockley stacking fault expansion in heavily nitrogen-doped SiC during high-temperature annealing," *J. Appl. Phys.* **124**, 025705 (2018).
- ⁴P. Fiorenza, M. S. Alessandrino, B. Carbone, C. Di Martino, A. Russo, M. Saggio, C. Venuto, E. Zanetti, F. Giannazzo, and F. Roccaforte, "Understanding the role of threading dislocations on 4H-SiC MOSFET breakdown under high temperature reverse bias stress," *Nanotechnology* **31**, 125203 (2020).
- ⁵H. Tsuchida, I. Kamata, T. Miyazawa, M. Ito, X. Zhang, and M. Nagano, "Recent advances in 4H-SiC epitaxy for high-voltage power devices," *Mater. Sci. Semicond. Process* **78**, 2–12 (2018).
- ⁶M. Na, J. Keum, J. H. Moon, and W. Bahng, "The effect of threading dislocation on current-voltage characteristics of 3.3 kV 4H-SiC Schottky barrier diode," *ECS Trans.* **85**(7), 59–65 (2018).
- ⁷H. J. Jung, S. B. Yun, J. H. Moon, W.-J. Kim, and W. Bahng, "Impact of stacking fault on the I-V characteristics of 4H-SiC Schottky barrier diode," *Mater. Sci. Forum* **821–823**, 563–566 (2015).
- ⁸S. Ha, P. Mieszkowski, M. Skowronski, and L. B. Rowland, "Dislocation conversion in 4H silicon carbide epitaxy," *J. Cryst. Growth* **244**, 257–266 (2002).
- ⁹T. Kimoto, "Material science and device physics in SiC technology for high-voltage power devices," *Jpn. J. Appl. Phys.* **54**, 040103 (2015).
- ¹⁰K. Wada, T. Terao, H. Itoh, T. Hori, H. Doi, M. Furumai, and T. Tanabe, "99.9% BPD-free 4H-SiC epitaxial layer with precisely controlled doping upon 3 × 150 mm hot-wall CVD," *Mater. Sci. Forum* **924**, 72–75 (2018).
- ¹¹N. Zhang, Y. Chen, Y. Zhang, M. Dudley, and R. E. Stahlbush, "Nucleation mechanism of dislocation half-loop arrays in 4H-silicon carbide homoepitaxial layers," *Appl. Phys. Lett.* **94**, 122108 (2009).
- ¹²X. Zhang, M. Skowronski, K. X. Liu, R. E. Stahlbush, J. J. Sumakeris, M. J. Paisley, and M. J. O'Loughlin, "Glide and multiplication of basal plane dislocations during homoepitaxy," *J. Appl. Phys.* **102**, 093520 (2007).
- ¹³X. Zhang, T. Miyazawa, and H. Tsuchida, "Critical conditions of misfit dislocation formation in 4H-SiC epilayer," *Mater. Sci. Forum* **717–720**, 313–318 (2012).
- ¹⁴M. Nagano, H. Tsuchida, T. Suzuki, T. Hatakeyama, J. Senzaki, and K. Fukuda, "Annealing induced extended defects in as-grown and ion-implanted 4H-SiC epitaxial layers," *J. Appl. Phys.* **108**, 013511 (2010).
- ¹⁵H. Jacobson, J. Birch, C. Hallin, A. Henry, R. Yakimova, T. Tuomi, E. Janzen, and U. Lindefelt, "Doping-induced strain in N-doped 4H-SiC crystals," *Appl. Phys. Lett.* **82**, 3689–3691 (2003).
- ¹⁶X. Zhang, S. Ha, Y. Hanlumnyang, C. H. Chou, V. Rodriguez, M. Skowronski, J. J. Sumakeris, M. J. Paisley, and M. J. O'Loughlin, "Morphology of basal plane dislocations in 4H-SiC homoepitaxial layers grown by chemical vapor deposition," *J. Appl. Phys.* **101**, 053517 (2007).
- ¹⁷H. Wang, M. Dudley, F. Wu, Y. Yang, B. Raghethamachar, J. Zhang, G. Chung, B. Thomas, E. K. Sanchez, S. G. Mueller, D. Hansen, and M. J. Loboda, "Studies of the origins of half-loop arrays and interfacial dislocations observed in homoepitaxial layers of 4H-SiC," *J. Electron. Mater.* **44**(5), 1268–1274 (2014).
- ¹⁸Y. Bu, H. Yoshimoto, N. Watanabek, and A. Shima, "Fabrication of 4H-SiC PiN diodes without bipolar degradation by improved device processes," *J. Appl. Phys.* **122**, 244504 (2017).
- ¹⁹N. Kaji, H. Niwa, J. Suda, and T. Kimoto, "Ultrahigh-voltage (>20 kV) SiC PiN diodes with a space-modulated JTE and lifetime enhancement process via thermal oxidation," *Mater. Sci. Forum* **779–780**, 832–835 (2014).
- ²⁰T. Kimoto and H. Watanabe, "Defect engineering in SiC technology for high-voltage power devices," *Appl. Phys. Express* **13**, 120101 (2020).
- ²¹J. H. Hubbell and S. M. Seltzer, "Tables of x-ray mass attenuation coefficients and mass energy-absorption coefficients from 1 keV to 20 MeV for elements Z = 1 to 92 and 48 additional substances of dosimetric interest," NIST Standard Reference Database 126, Dataset (2004). <https://doi.org/10.18434/T4D01F>
- ²²G. Feng, J. Suda, and T. Kimoto, "Characterization of stacking faults in 4H-SiC epilayers by room-temperature microphotoluminescence mapping," *Appl. Phys. Lett.* **92**, 221906 (2008).
- ²³S. Ha, H. J. Chung, N. T. Nuhfer, and M. Skowronski, "Dislocation nucleation in 4H silicon carbide epitaxy," *J. Cryst. Growth* **262**, 130–138 (2004).
- ²⁴J. L. Demenet, M. H. Hong, and P. Pirouz, "Deformation tests on 4H-SiC single crystals between 900 °C and 1360 °C and the microstructure of the deformed samples," *Mater. Sci. Forum* **338–342**, 517–520 (2000).
- ²⁵D. Hull and D. J. Bacon, *Introduction to Dislocations* (Elsevier, Burlington, MA, 2011).
- ²⁶K. Kamitani, M. Grimsditch, J. C. Nipko, and C.-K. Loong, "The elastic constants of silicon carbide: A Brillouin-scattering study of 4H and 6H SiC single crystals," *J. Appl. Phys.* **82**(6), 3152 (1997).